Bioactive Materials 50 (2025) 461–474

Contents lists available at ScienceDirect

Bioactive Materials

journal homepage: www.keaipublishing.com/en/journals/bioactive-materials

Cryopreservable, scalable and ready-to-use cell-laden patches for diabetic ulcer treatment

Bangrui Yu [a,b], Lanlan Peng [a,b], Wenjun Dang [a,b], Ying Fu [a,b], Zhijie Li [a,b], Jinteng Feng [c], Heng Zhao [c], Tian Wang [a,b], Feng Xu [a,b], Martin L. Yarmush [d,e], Haishui Huang [a,b,*]

[a] The Key Laboratory of Biomedical Information Engineering of Ministry of Education, Xi'an Jiaotong University, Xi'an, Shaanxi, 710049, PR China
[b] Bioinspired Engineering and Biomechanics Center (BEBC), School of Life Science and Technology, Xi'an Jiaotong University, Xi'an, Shaanxi, 710049, PR China
[c] Department of Thoracic Surgery, The First Affiliated Hospital of Xi'an Jiaotong University, Xi'an, 710049, PR China
[d] Center for Engineering in Medicine and Surgery, Massachusetts General Hospital, Harvard Medical School and Shriners Hospitals for Children, Boston, MA, 02114, United States
[e] Department of Biomedical Engineering, Rutgers University, Piscataway, NJ, 08854, United States

A B S T R A C T

Stem cell-laden hydrogel patches are promising candidates to treat chronic ulcers due to cells' long-lasting and dynamic responses to wound microenvironment. However, their clinical translations are prohibited by the cryopreservation difficulty due to their weak mechanical strength and slow biotransport capability, and by the morphological mismatch between clinical ulcers and pre-fabricated patches. Here we report a stem cell-laden alginate-dopamine hydrogel patch that can be readily cryopreserved, processed, and scaled toward clinical usages. This cell-hydrogel patch not only maintains cell viability and structure integrity during cryopreservation, but also can be directly utilized without centrifugation or incubation post cryopreservation. In addition, this tissue-adhesive hydrogel patch enables close wound contact and fast cellular response, and its scalable and flexible structure enables assembly for large or irregularly shaped ulcers. Therefore, it accelerates ulcer healing and reduces scar formation *via* continuous, versatile, self-adjusting paracrine of imbedded, cryopreserved stem cells. These findings highlight its potential for scalable clinical applications in chronic wound management and pave the way for broader adoption of ready-to-use regenerative therapies.

1. Introduction

Mesenchymal stem cell is a promising treatment for notorious diabetic ulcers due to its long-lasting ability of immunomodulation, angiogenesis regulation, and wound re-epithelialization [1,2]. Its clinical translation is severely challenged by low cell implantation efficiency and survival rate in the diabetic ulcers because of cell leakage, migration, and the complex and hostile inflammatory microenvironment in the lesion [3–5]. To improve cell retention and survival rate, biocompatible hydrogels laden with stem cells is an effective strategy [6–8]. The hydrogel carrier can not only maintain cell activity and function, evade the host's immune rejection, but also prevent stem cells from migrating and leaking into the lesion [9,10]. In addition, cell-laden hydrogels should be cryopreserved *in vitro* to bridge the spatiotemporal gap between the preparation and application destinations for clinical applications [11].

However, the cryopreservation of cell-laden hydrogels is challenged by the dilemma of its weak mechanical strength and slow heat and mass transfers, especially for macroscale ones. Cryopreservation *via* traditional slow-freezing requires cells to dehydrate and deform to minimize intracellular ice formation (IIF) and utilizes penetrating cryoprotectant (*p*CPA, e.g. 10 % dimethyl sulfoxide (DMSO)). However, while DMSO is effective in protecting cells during freezing, it can impair cellular activity, induce phenotypic changes in stem cells, and cause severe adverse effects (e.g., nausea, vomiting, and even cardiac arrest) in patients [12–14].Large constructs impede heat and mass transfers in cryopreservation, exacerbating thermal stress to cause structure crack and demanding trained practitioners and specialized personnel and equipment (such as centrifuges, safety cabinets, and incubators) to remove CPAs before usage [15]. Cryopreservation *via* vitrification without ice crystal formation has been achieved to preserve stem cells, but it is only applicable to microcapsules as it requires fast cooling/warming and high CPA concentrations [16–18]. As a result, the current preservation approach for macroscale cell-sheets or cell-laden constructs is hypothermic storage around 4 °C without phase transition, but the storage period is short (usually <1 week) due to high temperatures [19–21].

On the other hand, 1,2-propanediol (PROH), has been recently

Peer review under the responsibility of editorial board of Bioactive Materials.
* Corresponding author.School of Life Science and Technology, Xi'an Jiaotong University Xi'an, Shaanxi, 710049, PR China.
E-mail address: haishuihuang@xjtu.edu.cn (H. Huang).

https://doi.org/10.1016/j.bioactmat.2025.04.024
Received 18 January 2025; Received in revised form 27 March 2025; Accepted 19 April 2025

identified as a safe alternative or supplement to DMSO due to its reduced cytotoxicity (i.e., it can be used as a food additive) [22]. By reducing the required concentration of DMSO, PROH minimizes the associated toxicity and osmotic damage. Moreover, PROH also protects cells from the rigors of osmotic pressure, leading to enhanced cell preservation [23]. In addition, non-penetrating CPAs (*n*CPAs, e.g. trehalose) with minimum cytotoxicity can improve cryopreservation as they pre-dehydrate cells before freezing, stabilize cytoplasmic membranes, and regulate nucleation and propagation of ice crystals [24,25]. Therefore, a cryopreservation method for macroscale cell-laden constructs should be developed by comprehensively considering CPA cytotoxicity, CPA removal, and structural integrity.

In addition, clinical diabetic ulcers usually have unpredictable size and shape, challenging the pre-design and pre-fabrication of wound dressings [26]. Traditional dressings are laden with particular biochemical molecules, which are required to cover the whole lesion to deliver specific protection and therapeutic effects [27]. The passive, autonomous release of therapeutic molecules from dressings is usually at an exponentially decreased rate, leading to frequent replacement of wound dressings and associated secondary injuries [28,29]. On the contrary, stem cell hydrogel can continually release regulatory cytokines as long as cell maintains viable, functional, and close contact to wound microenvironment [30,31]. Therefore, tissue adhesive patches could be assembled to treat large, irregular-shaped ulcers, and the paracrine secretion of imbedded stem cell even could treat uncovered regions of ulcers.

Here, we describe a cryopreservable and scalable macroscale adipose-derived stem cell (ADSC)-laden alginate-dopamine hydrogel patch (Alg-DA, diameter: 10 mm, thickness: 1 mm) patch toward clinical treatment of diabetic ulcers. The thin cell-laden patch can be cryopreserved with a CPA cocktail of DMSO, PROH, and trehalose, maintaining patch structural integrity, cell viability, and functions. Importantly, cell-laden patches can be used immediately after thawing without the need for centrifugation or prolonged incubation, offering a practical "ready-to-use" solution for immediate clinical application. In addition, the stem cells within this tissue-adhesive patch keep close contact to the diabetic wound, and thus, accelerate diabetic wound healing and reduce scar formation by dynamically regulating inflammation, angiogenesis, re-epithelialization, and collagen deposition. Furthermore, the scalable and flexible design of this patch can be arrayed to treat large or irregularly shaped ulcers in clinical settings, thereby significantly simplifying clinical workflows and providing a practical and efficient therapeutic solution for diabetic wound care on demand.

2. Materials and methods

2.1. Synthesis of alginate-dopamine

Alginate-dopamine was synthesized by amidation reaction using N-(3-dimethylaminopropyl)-N-ethylcarbodiimide hydrochloride (EDC) and N-hydroxysuccinimide (NHS) [32]. Specifically, alginate (2 % w/v) was dissolved in 100 ml of MES buffer (100 mM, pH = 5.6). After stirring overnight at room temperature, 5 mM EDC and NHS were added to the alginate solution. After mixing for 30 min, 10 mM dopamine hydrochloride was added to the above solution and stirred for 24 h at room temperature under N_2 protection. Finally, the reaction mixture was dialyzed with deionized water (Molecular weight cut-off 6–8 kDa) for three days. The resulting product was then freeze-dried. The successful synthesis of alginate-dopamine was confirmed by UV–Vis spectroscopy (Lambda 35, PerkinElmer, USA) and ^{1}H NMR spectroscopy (600 MHz, Burker, Switzerland).

2.2. Fabrication of ADSC-patch

The fabrication process of ADSC-patches is shown in Fig. S1A. PMMA was cut into 10 mm diameter discs by a laser engraving machine (Universal VLS2.30, USA) and fixed on a Petri dish (Thermo Fisher, USA) to obtain a master mold. Then, the negative mold was obtained by replicating the master mold by PDMS. Specifically, PDMS (the ratio of substrate to curing agent is 10:1, Dow Corning) is poured on the master mold, vacuum degassed for 30 min, then cured at 60 °C overnight, and finally demolded. The obtained PDMS molds were autoclaved for the preparation of ADSC-patches. Next, SD rat ADSCs (P4-P6, Cyagen) were resuspended in 2 % (w/v) hydrogel precursor solution (Alg or Alg-DA dissolved in DMEM) and the resulting mixture was added dropwise into PDMS molds (87.5 μL/per hole), then the molds were covered uniformly with dialysis membrane, and finally an appropriate amount of 100 mM $CaCl_2$ solution was added dropwise on top of the dialysis membrane. After cross-linking at 37 °C for 10 min, the dialysis membrane was gently peeled off to obtain an appropriate amount of uniform cell-laden patch.

Furthermore, PDMS molds with the same diameter and different thicknesses (0.5, 0.75, and 1 mm) were used to prepare hydrogel patches of the corresponding thicknesses, respectively, to assess the impact of thickness on the integrity of hydrogel patches during demolding, cryopreservation (using 10 % DMSO or a combination of 5 % DMSO and 5 % PROH), and thawing.

2.3. Characterization of ADSC-patch

The lap-shear test was used to evaluate adhesion strength. Specifically, alginate hydrogel (Alg) and alginate-dopamine hydrogel (Alg-DA) were applied to the adhesive area of two cleaned pig skin specimens (10 × 50 mm) and subjected to constant pressure to ensure full interfacial contact. The bonded specimens were fixed in a tensile machine, and shear force was applied at a constant rate until complete interfacial failure occurred, at which point the maximum shear stress was recorded and adhesion strength was calculated. To evaluate the adhesion and flexibility of the hydrogel patch before and after cryopreservation, the hydrogel patch before (labeled with methylthioninium chloride) and after cryopreservation (labeled with rhodamine) was placed on the finger joint, and its adhesion was evaluated by observing the patch during finger flexion. In addition, a 10 mm diameter wound was created on the back of SD rats. The hydrogel patch, stained with rhodamine, was applied to the wound, and the adhesion of the patch to the wound was observed by gently rotating the rat to evaluate the patch's stability. The ADSC-patch was weighed and placed in HBSS, then incubated in a constant temperature shaker (37 °C at 60 rpm), and samples were taken at fixed time points to observe the *in vitro* degradation of the patch. Finally, hydrogel patches before and after cryopreservation were stored at −20 °C overnight and subsequently freeze-dried. After gold coating, cross-sections of the hydrogels were examined using field emission scanning electron microscopy (GeminiSEM, ZEISS, Germany) to assess their microstructure.

Long-term viability and biocompatibility of ADSCs in hydrogel patches were assessed using the LIVE/DEAD cell viability assay kit (Thermo Fisher, USA) following the manufacturer's instructions. Briefly, cell-laden patches were incubated at 37 °C for more than 7 days, rinsed twice with HBSS (Hank's Balanced Salt Solution), and then stained with HBSS containing 5 μM calcein AM and 5 μM ethidium homodimer (Invitrogen), respectively, to distinguish between live and dead cells. After incubation for 20 min at 37 °C in the dark, the live cells (green) and dead cells (red) were observed and quantified using fluorescence microscopy to assess cell viability. Moreover, apoptosis was assessed in both normal culture conditions and in cell-laden hydrogel patches using the Tunel Apoptosis Kit (Roche, Switzerland) according to the manufacturer's instructions.

2.4. Cryopreservation protocol

Pre-add 0.5 M trehalose (Sigma) to the hydrogel precursor solution

to obtain ADSC-patch containing trehalose. The loading of trehalose can predehydrates the cells, thereby inhibiting the formation of intracellular ice during cryopreservation [24]. Subsequently, the ADSC-patches (with or without trehalose) are suspended in a frozen storage tube containing 1 ml of *p*CPA solution (10 % DMSO, 5 % DMSO + 5 % PROH, 10 % PROH) and then left to stand at 4 °C for 30 min to ensure complete penetration of *p*CPA into the cells to achieve internal and external equilibrium. Next, the frozen storage tubes are placed in a Mr. Frosty™ Freezing Container pre-cooled at 4 °C and then transferred to −80 °C for overnight. This freezing vessel will cool the ADSC-patch in a gradient of 1 °C/min. Finally, freeze tubes are placed in LN_2 for long-term storage.

After cryopreservation of the ADSC-patches for at least 1 week, they were removed from the LN_2 and immediately rewarmed in a 37 °C water bath until completely thawed (no more than 2 min). The ADSC-patch was then removed from the frozen storage tube and placed in a 35 mm Petri dish (Thermo Fisher) containing 5 mL of DMEM medium (Hyclone) and washed for various times (5-, 15- and 30-min) to remove as much toxic *p*CPA (especially DMSO) as possible. Finally, the ADSC-patches were used directly for subsequent experiments (Cryo ADSC-patch) or incubated at 37 °C for 24 h to recover (Optional) and then used for subsequent experiments (Cryo/rec ADSC-patch).

2.5. Characterization of cryopreserved ADSC-patches

An Anton Paar rheometer (MCR 302, Austria) was used to perform the rheological tests. Hydrogel patches (fresh and cryopreserved, where CPA was: 10 % DMSO or 5 % DMSO + 5 % PROH respectively) were placed between parallel plates with a diameter of 10 mm and a gap height of 1 mm. Angular frequencies were scanned from 0.1 to 10 rad/s at a strain of 0.5 %. Finally, the storage and loss moduli were calculated by averaging the moduli between frequencies of 0.25 and 2.5 rad/s. To determine the optimal cryopreservation conditions for the ADSC-patches, the viability of ADSCs under different CPA combinations and wash time conditions was determined by a LIVE/DEAD Cell Vitality Assay Kit.

High performance liquid chromatography (HPLC, UltiMate 3000, Thermo, USA) was used to measure the concentration of DMSO residues after 15-min of wash and 24-h incubation. Briefly, a C18 analytical column was selected as the separation column and maintained at 40 °C. The mobile phase was methanol: water = 20:80 with a flow rate of 0.8 mL/min and an injection volume of 5 μL. First, standard concentrations (0.01 %, 0.025 %, 0.05 %, 0.25 %, 0.5 %) of DMSO solutions were prepared using HBSS as the solvent and the DMSO standard curve was measured. Next, the samples were analyzed using HPLC and the residual DMSO concentrations in the ADSC-patches were calculated.

To systematically evaluate the *in vitro* cytotoxic effects of residual DMSO, Raw264.7, NIH/3T3, and HUVECs. were inoculated into 96-well plates with different DMSO concentrations (consistent with residual levels of CPA#1 and CPA#2). After incubation at 37 °C for 24 h, cell viability was assessed using the CCK8 assay following the manufacturer's instructions.

2.6. Stemness and functional tests of ADSC

For immunostaining of CD44 (positive) and CD34 (negative) receptors, ADSC-patches were placed on confocal dishes (Thermo Fisher), washed with HBSS and fixed with 4 % paraformaldehyde. The fixed samples were incubated in 1 % BSA at room temperature for 1h to block potential non-specific binding, and then incubated overnight at 4 °C with primary antibody for CD44 (Abcam) or CD34 (Abcam) according to the manufacturer's instructions. Afterward, the samples were washed 3 times with HBSS and incubated with diluted secondary antibody (1:50 dilution) at room for temperature and protected from light. Finally, the samples were washed and the nuclei were stained with DAPI and visualized by confocal microscopy (Olympus, Japan). To assess the gene expression levels of ADSCs before and after cryopreservation, qRT-PCR analysis was used to quantify the expression of three stem cell pluripotency gene markers: KIf4, Nanog, and SOX-2. Released ADSCs were collected by lysing ADSC-patches with 70 mM trisodium citrate and washed twice with PBS. Total RNA was isolated using Trizol (Solarbio) and then reverse transcribed using the RevertAid First Strand cDNA Synthesis Kit (Thermo Fisher) according to the manufacturer's instructions. Next, qRT-PCR analysis was performed using a 7500 Fast real-time PCR system (AppliedBiosystems, Thermo). Relative gene expression was calculated using the $2^{-\Delta\Delta Ct}$ method, and expression was normalized using 3-phosphoglyceraldehyde dehydrogenase as the housekeeping gene. The primer sequences are shown in Table S1 [33].

To assess metabolic changes before and after cryopreservation, cryopreserved and non-cryopreserved ADSC-patches were incubated in 1 mL of medium for 24 h. The culture medium was collected, and glucose and lactate levels were quantified using a blood gas analyzer. Additionally, ATP content in ADSCs was measured using the CellTiter-Glo 3D Cell Viability Assay (Promega) according to the manufacturer's instructions. Next, ADSC-patches cultured for 24 h before and after cryopreservation were collected. The hydrogel was lysed to release encapsulated cells, which were subsequently processed using the Cell Cycle Detection Kit (Elabscience) according to the manufacturer's instructions. Cell cycle changes were then analyzed by flow cytometry.

The effect of ADSC-patch on cell migration (HUVECs and NIH/3T3) capacity was measured using 24-well Transwell plates (Corning) with 8-μm pore-size filters. Briefly, HUVECs or NIH/3T3 was inoculated into the upper chamber at a density of 2×10^4, and then the ADSC-patch was placed in the lower chamber. After incubation at 37 °C for 24 h, the cells were fixed with 4 % paraformaldehyde, the cells remaining on the upper surface of the filter membrane were gently removed with a cotton swab, and the migrated cells on the lower surface of the filter membrane were stained with 0.1 % crystal violet solution for 10 min. The migrated cells were photographed with a fluorescence microscope, and the cell migration data were analyzed using imageJ. For angiogenesis assays, thawed matrigel (Corning) was added to pre-cooled transwell plates and incubated at 37 °C for 30 min to cure. Then, HUVEC were seeded with 1×10^5 cells per well into the lower chamber and hydrogel patches are added to the upper chamber. After co-incubation at 37 °C for 6 h, endothelial tube formation was observed using inverted fluorescence microscopy and quantified by ImageJ.

Expression of M1 and M2 macrophage marker genes (including iNOS2, Arg-1, IL-6, IL-10, IL-1β, and TNF-α, with β-actin used as a housekeeping gene) was assessed by qRT-PCR analysis. Briefly, Raw264.7 cells (5×10^4/per well) were inoculated in the lower chamber of Transwell plates. After overnight incubation, the cells were stimulated with LPS (1 μg/mL) for 24 h to induce polarization of M1 phenotype macrophages. Then, hydrogel patches were added to the upper chamber and after co-incubation at 37 °C for 24 h, collected RAW264.7 cells, extracted total RNA by Trizol, and analyzed macrophage mRNA expression levels by qRT-PCR. The primer sequences are listed in Table S2 [34].

2.7. Establishment of a diabetic wound model

All experimental procedures involving animals were approved by Xi'an Jiaotong University, School of Life Science and Technology (Xi'an, China). As previously reported [35], male SD rats weighing approximately 180–220 g were used to induce a type 1 diabetes model. Rats were fasted overnight followed by a single intraperitoneal injection of 70 mg/kg of streptozotocin (STZ). 2 weeks later, blood glucose was measured and rats with sustained blood glucose levels above 16.7 mM accompanied by weight loss and polyuria were considered to have diabetes. Subsequently, two full-thickness wounds were constructed on the back of the rats. Briefly, rats were anesthetized with 2 % sodium pentobarbital, their dorsal hair was shaved, and two full-thickness wounds (diameter:10 mm) on the dorsal skin were created for rats using a biopsy punch.

2.8. In vivo bioluminescence imaging

Lentiviral vectors (Cyagen) containing luciferase$^+$ (Luc)/green fluorescent protein$^+$ (GFP) were transfected into ADSCs for *in vivo* bioluminescence imaging. Specifically, ADSC were inoculated onto six-well plates (Thermo Fisher), transfected with lentivirus (MOI = number of lentivirus/number of cells = 30) for 8 h after reaching 30–50 % confluency, and then screened by replacing the lentiviral medium with medium containing puromycin. After 48–72h, expression of green fluorescent protein was observed under inverted fluorescence microscopy, indicating successful transfection. Next, diabetic rats with open wounds were treated with Luc$^+$/GFP$^+$ ADSCs, and were randomly divided into three groups: ADSC, Fresh ADSC-hydrogel patch and cryopreserved ADSC-hydrogel patches (Cryo ADSC-patch), and then fluorescein was injected at the wound site and imaged using an *in vivo* imaging system on days 0, 3, 5 and 7 (Vieworks, Smart-LF, Korean).

2.9. Treatment of diabetic ulcers

Diabetic rats with uniform ulcers were randomly divided into six groups: untreated controls (control, covered with 3M Tegaderm™ only), treated with hydrogel (Alg-DA) or ADSCs (ADSC) alone, and treated with hydrogel patches before and after cryopreservation (ADSC-patch, Cryo ADSC-patch, Cryo/rec ADSC-patch) (n = 18). The wounds were treated with different conditions and then fixed with Tegaderm and gauze cover. Notably, in the control group, Tegaderm™ alone was applied without additional treatment, serving as a positive control, as it is commonly used in clinical and preclinical studies to facilitate wound healing. To monitor wound closure, digital images of the wounds were acquired on days 0, 3, 7, 9, 12, and 14, and the wound size was determined using ImageJ.

To further evaluate the therapeutic efficacy of the Cryo-ADSC patch in diabetic ulcers, rats were randomly assigned to two groups, with wounds covered by either the Cryo-ADSC patch or the commercial Algisite™ dressing. Digital images of the wounds were taken on days 0, 3, 7, 9, 12, and 14, and wound size was quantified using ImageJ. Additionally, H&E staining was conducted to evaluate wound healing quality.

2.10. Histological analysis and protein analysis

Traumatic tissues from rats were collected on days 3, 7 and 14 for histological and protein analysis, respectively. For protein analysis, a double antibody sandwich enzyme-linked immunosorbent assay (ELISA, Elabscience) was used to analyze wound cytokine levels. Briefly, after removing residual blood or impurities from the wound, pre-cooled PBS (1:9 weight-to-volume ratio) was added, thoroughly homogenized on ice using a tissue homogenizer, centrifuged, and the supernatant collected. Then, the expression levels of VEGF, TNF-α, IL-6, IL-10 and TGF-β1 at the wound were analyzed by ELISA kits according to the manufacturer's instructions. The homogenized wound tissues were processed for protein quantification using the BCA kit, followed by Western blot (WB) analysis to detect VEGF and TNF-α (Thermo) expression in wound tissues through electrophoresis, membrane transfer, blocking, primary antibody incubation, and HRP-conjugated secondary antibody detection. Finally, the cytokine levels in the wounds were calculated according to the cytokine standard curve.

For histological analysis, trauma tissue was fixed in 4 % paraformaldehyde, embedded in paraffin, and sectioned. H&E and Masson staining were performed according to the manufacturer's instructions to assess wound-specific healing and collagen deposition. Immunohistochemical staining (IHC) for Col3, CD68, CD163, and CD31 (Abcam) was performed at the wound site to assess the wound healing mechanism. Briefly, after deparaffinization, quenching of endogenous peroxidase activity, antigen retrieval, and blocking, the sections were incubated with primary antibodies overnight at 4 °C and then incubated with the corresponding secondary antibodies for 2 h at room temperature. Cell nuclei were stained with DAPI. Quantitative analysis of the staining results was performed using ImageJ.

2.11. Construction and treatment of large-scale diabetic wounds

To test the applicability of hydrogel patches for large irregular ulcers, a 2 × 3 cm oversized full-length wound model was constructed in the central dorsal region of diabetic rats. The Rats were randomly divided into three groups: control, Alg-DA and Cryo ADSC-patch (n = 3). Among them, 8 hydrogel patches were covered on the wound on the day of surgery, and then the appropriate number of hydrogel patches were placed according to the actual size of the wound as it closed. Finally, the wound healing rate and scar area were calculated by Image J software. In addition, wound tissue was collected at 35 days and further assessed for wound healing by H&E staining. In addition, Masson's staining and immunohistochemical staining for CD68, CD163, collagen type I (Col 1) (Proteintech) and collagen type III (Col 3) (Affinity) were performed on wound tissues to evaluate wound healing quality.

2.12. Statistical analysis

All analytical determinations were performed at least in triplicate (n $\geq$ 3). Results were expressed as mean ± standard deviation (SD). One-way analysis of variance (ANOVA) and two-tailed Student's *t*-test were used to determine statistical significance. The values of * ($p < 0.05$), ** ($p < 0.01$), and *** ($p < 0.001$) were considered statistically significant.

3. Results

3.1. Fabrication of thin ADSC-patch

ADSC-laden alginate hydrogel patches (ADSC-patch) were prepared in PDMS molds fabricated using PMMA (Fig. S1A). Cell-laden hydrogel precursor solution without serum was injected into PDMS molds, covered by a semi-permeable dialysis membrane, and crosslinked (10-min) into hydrogel *via* the diffusion of Ca^{2+} from overhead $CaCl_2$ solution. A 10-min diffusion crosslinking obtains hydrogel patches with high mechanical strength without causing substantial cell injuries/death. Notably, the PDMS mold can be reused and the overall time of one production cycle is less than 15 min, which enables the economical mass-production of patches. To maintain close contact to and prevent displacement in wound bed, tissue adhesiveness of hydrogel patches is strongly required. Inspired by the strong adhesion of marine mussels in humid environments [36], dopamine (DA), which increases hydrogel adhesion and cell affinity [37,38], is grafted onto the alginate through carbodiimide coupling (EDC/NHS) as evidenced by ultraviolet–visible light absorption and ^{1}H nuclear magnetic resonance (^{1}H NMR) (Fig. 1A and S1B). Next, Lap-shear adhesion tests using porcine skin as a model substrate demonstrated that dopamine modification significantly improved the tissue adhesion capacity of the hydrogel patch (Fig. S1C), which is crucial for maintaining stable contact between the dopamine-alginate hydrogel patch (Alg-DA) and the wound site. Moreover, Alg-DA not only retained the pancake shape of the mold, but also adhered closely to the skin without shrinking or shifting before and after cryopreservation (closely attaching to curving digital joints as seen in Fig. 1B), providing tissue adhesion, flexibility and compliance. In addition, the rat model further demonstrated the adhesion of the hydrogel patch to the wound (Fig. S1D).

Notably, the "egg carton" structure of Alg-DA hydrogel [39], cross-linked by Ca^{2+}, not only effectively stabilized the encapsulated ADSCs, preventing cell loss, but also ensured high biocompatibility, which avoided apoptosis and maintained consistently high cell viability for over 7 days (Fig. 1C, D and S1E, F). In addition, the ADSC-patch remains structurally stable *in vitro* over an extended period (only 6.14 ± 1.30 % degraded in 21 days) (Fig. S1G), effectively preventing cell

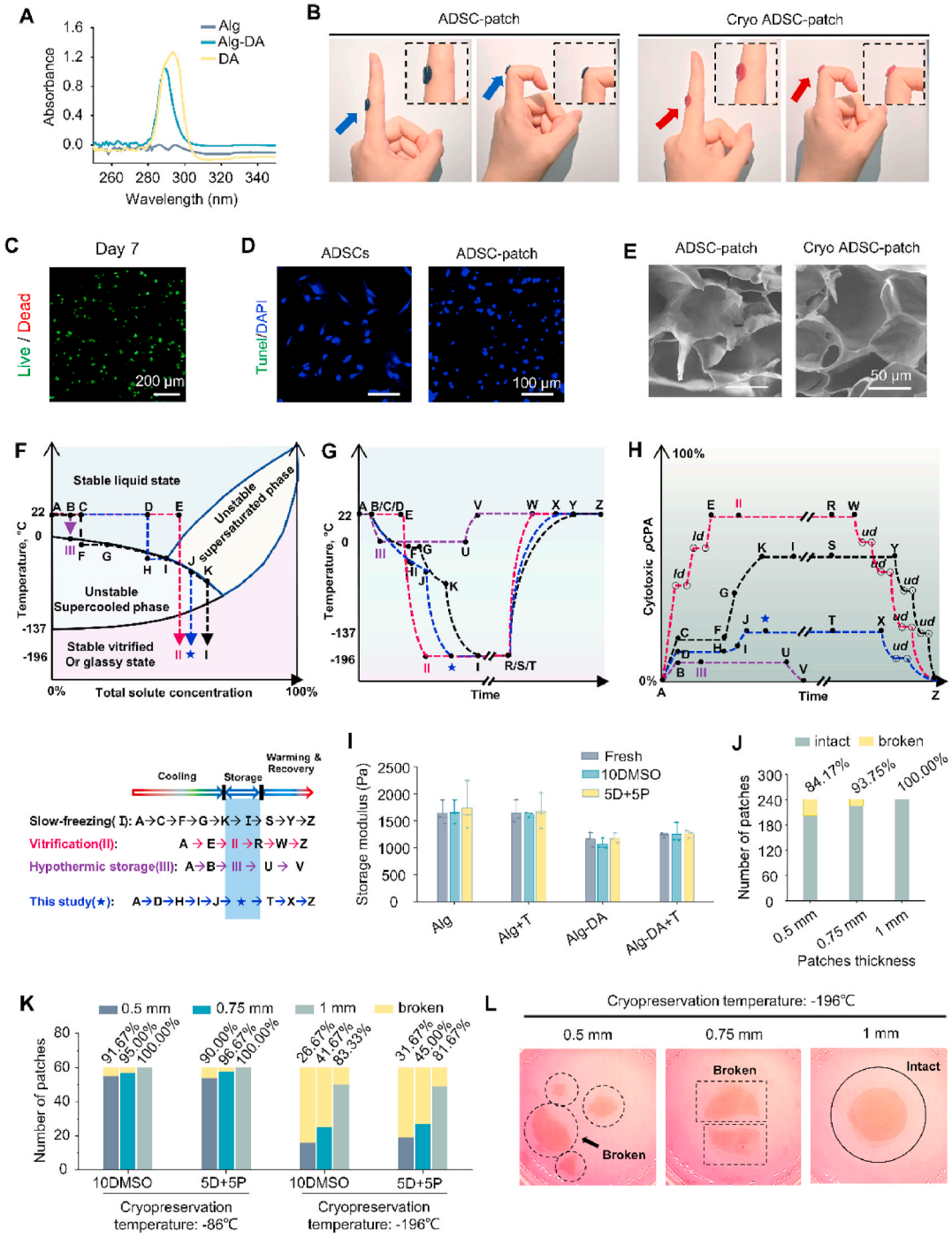

Fig. 1. Fabrication, cryopreservation and structure maintenance of ADSC-patch. (**A**) UV–vis spectrum of synthesized Alg-DA. (**B**) Adhesion of ADSC-patch to outstretched finger and digital joint. Methylthioninium chloride labeled ADSC-patch before cryopreservation, rhodamine labeled ADSC-patch after cryopreservation. (**C**) ADSCs viability in Alg-DA hydrogel patches on Day 7. ADSC-patch and Cryo ADSC-patch refers to fresh ADSC-patch and cryopreserved ADSC-patch, respectively. (**D**) Tunel staining of ADSCs in normal culture and ADSC-patches to characterize apoptosis. (**E**) SEM images of ADSC-patches before and after cryopreservation. Comparisons of cryopreservation pathways between this study and other conventional approaches in (**F**) phase diagram, (**G**) thermal time course, and (**H**) cytotoxic (penetrating CPA, *p*CPA) time course. *ld* and *ud* represent CPA loading and unloading steps before and after cryopreservation, respectively. Arrows indicate the direction of the preservation process. The axes are not drawn to scale. The rates of temperature and osmolality change are represented by the slopes of the curves. Long-term storage is denoted by '//'. (**I**) Storage modulus of various hydrogel patches before and after cryopreservation. (**J**) Statistics on structural integrity of 0.5 mm, 0.75 mm and 1 mm thick hydrogel patches after fabrication. (**K**) Statistics on structural integrity of 0.5 mm, 0.75 mm and 1 mm thick hydrogel patches after cryopreservation in −86 °C and in LN_2 (−196 °C). (**L**) Representative images of 0.5 mm, 0.75 mm and 1 mm thick hydrogel patches after cryopreservation in LN_2 (−196 °C). 10 DMSO and 5D+5P represent cryopreservation with 10 % DMSO and 5 % DMSO+5 % PROH, respectively. The dashed line represents the broken ADSC-patch, while the solid line represents the intact ADSC-patch Independent repeat experiment n ≥ 3. *: $p < 0.05$, **: $p < 0.01$, and ***: $p < 0.001$.

leakage while maintaining robust cell support. Moreover, the porous microstructures of Alg-DA hydrogel patches remain largely unaltered following cryopreservation, as evidenced by scanning electron microscopy (SEM), with porosity remaining consistent before and after cryopreservation (Fig. 1E and S1H, I).

3.2. Cryopreservation of macroscale ADSC-patch

Macroscale ADSC-patches are cryopreserved following A→D→H→I→J→★→T →X →Z in Fig. 1F-H by developing a hybrid CPA that combines *p*CPA (DMSO, PROH) and *n*CPA (trehalose) (Fig. 1). Post cryopreservation, ADSC-patches are transferred to DMEM for one-step washing to remove *p*CPA (Fig. 1H), and to a 37 °C incubator for cell recovery (optional). Pre-dehydration with trehalose reduces intracellular ice formation (IIF) during cryopreservation, thereby preventing cell damage [24]. Thus, trehalose would predehydrate cell prior cryopreservation, reducing osmotic shock and freezing concentration in conventional slow-freezing (H→I→J VS. F→G→K in Fig. 1F and H). Thin patches enable high warming rate to reduce ice recrystallization and cellular damages during thawing (T→X VS. S→Y in Fig. 1G). Compared to vitrification, this study relieves the stringent requirements of high CPA concentration (Point D VS. E in Fig. 1F–H) and ultrafast cooling/warming rates (J→★ VS. E→II and T→X VS. R→W in Fig. 1G). In addition, it reduces cytotoxic *p*CPA concentration (Point D VS. C VS. E in Fig. 1H) and enables one-step removal post cryopreservation (X→Z VS. Y→Z VS. W→Z in Fig. 1H). Compared to hypothermic storage, cryopreservation in −86 °C mechanical freezers or −196 °C liquid nitrogen of ADSC-hydrogel patches enables them to be stored for much longer time (★→T VS. III→U in Fig. 1G).

Sheet structures are facultative for biotransports in hydrogel gelation, cryopreservation, and wound treatments, because they facilitate heat and mass transfer in cryopreservation and allow close cell contact and rapid bioreactivity. Notably, a balance between hydrogel patch thickness and its preservation must be carefully considered. Thinner patches enhance the efficiency of heat and mass transfer, which is particularly advantageous during cryopreservation, whereas thicker patches may hinder the rate of cooling and warming, leading to potential thermal stress and ice formation. However, thinner patches are susceptible to fracture even fragmentation during mold stripping, transportation, and cryopreservation due to weak mechanical strength. The storage modulus of various hydrogels are measured by rheology (Fig. 1I), and the slight decrease in Alg-DA hydrogels is due to the possible interference of dopamine with the self-organization and interchain conformation of calcium present [38]. Notably, the low loss modulus (Fig. S1J) (relative to the storage modulus) indicates the predominantly elastic nature of the hydrogel, which is crucial for maintaining structural integrity during cryopreservation and ensuring stable adherence to the wound site. To obtain thinnest patches with intact structure, 0.5 mm-, 0.75 mm-, and 1 mm-thick patches are fabricated with 84.17 %, 93.75, and 100 % intact structure rate (ISR), respectively (Fig. 1J). Furthermore, the ISRs of patches with varying thicknesses were observed after cryopreservation with 10 % DMSO or 5 % DMSO +5 % PROH at −86 °C (short-term storage) and at −196 °C in LN_2 (long-term storage). The 1 mm-thick patches consistently exhibited higher ISRs, whereas thinner patches, particularly those stored in LN_2, showed lower ISRs (<45 %) (Fig. 1K and L). This can be attributed to the fact that thinner patches, due to their more fragile structure, are more susceptible to thermal stresses and physical shocks induced by temperature changes, often leading to fragmentation. Therefore, patch integrity is primarily influenced by thickness rather than by the composition of the CPA. 1 mm-thick Alg-DA patch is chosen to balance structural integrity and biotransport capability. Overall, the 1 mm thickness optimizes the robustness and clinical utility of cryopreservation. Its mechanical compliance prevents secondary damage, while rapid nutrient diffusion supports ADSC survival, which is essential for chronic wound therapies requiring prolonged biological activity.

The ultimate goal of cryopreservation is to preserve and extend the life and function of biologically active materials [11]. So, CPA cocktails of 10 % DMSO, 5 % DMSO+5 % PROH (5D + 5P) and 10 % PROH are trialed with 70.64 ± 4.09 %, 68.99 ± 2.92 %, and 59.18 ± 4.36 % cell viability, respectively (Fig. 2A and B), indicating DMSO and DMSO + PROH are better than PROH alone given the same total pCPA concentration. In contrast, the survival rate of ADSC-patch directly cryopreserved was only 14.94 ± 2.82 %. Notably, the survival rate of non-permeable trehalose alone was 33.51 ± 6.51 %, suggesting that prehydration alone was insufficient to completely mitigate cryoinjury in the absence of pCPA for ADSC-patches (Fig. 2A and B). However, cell viability significantly improved when trehalose was combined with a pCPA solution (Fig. 2A and B). Therefore, an optimal CPA cocktail can be reached (0.5M trehalose+5 % DMSO+5 % PROH, CPA #2) since it has much higher cell viability (90.90 ± 5.18 %) than 0.5M trehalose + 10 % DMSO combination (CPA #1, 77.25 ± 2.92 %).

At the user end, ease and flexible operation is critical for its widespread application. Cytotoxic *p*CPA (particularly DMSO) in patches need to be removed before implantation, which usually requires multistep washing, centrifugation, and incubation. Next, the elution time for a single use was optimized to ensure the safe and effective application of the cell-laden patch (Fig. 2C). After 5-, 15-, or 30-min wash, CPA #2 results in significantly higher cell viability than CPA #1 (Fig. 2D and S2A). In addition, 37 °C incubation of washed patches improves cell viability as dormant cells and sub-lethal cryoinjuries could gradually recover during incubation [40], especially CPA #2 washed for 15 min with a cell viability of 91.75 % (Fig. 2D and S2B). Moreover, 15-min wash is preferential regardless of wash temperatures (4 °C or 37 °C) (Fig. S3A). Extended incubation for 72 h confirmed that CPA #2 consistently outperformed CPA #1, as residual DMSO from CPA #1 adversely affected cell viability (Fig. 2E and S3B). Moreover, CPA#2 can also be used directly for cryopreservation of ADSCs, with cell viability up to 92.49 ± 2.09 % for ADSC without centrifugation (Fig. S3C and D).

Residual DMSO in ADSC-patches after 15-min wash and 24-h incubation are measured by HPLC (Fig. S4), Which are 0.08 ± 0.01 % and 0.016 ± 0.003 % for CPA #2, and 1.59 ± 0.25 % and 0.10 ± 0.01 % for CPA#1 (Fig. 2F). Thus a 15-min wash of CPA #2 achieves an equilibrium between ADSC-patches and wash solution (equilibrium concentration ~0.086 %), but not for CPA #1 (equilibrium concentration ~0.17 %). Since 0.1 % is generally regarded as the DMSO toxicity threshold [41], a 15-min wash of CPA #2 is sufficient to reduce DMSO to nontoxic level, and an extended 30-min wash would increase cell injury by exposure to cytotoxic level of DMSO (Fig. 2D). This further confirms the significant downregulation of cell viability in ADSC-patch cryopreserved with CPA #1 after 72 h culture (Fig. 2E). Furthermore, we have included additional *in vitro* cytotoxicity analyses using Raw264.7, NIH/3T3, and HUVECs. A residual DMSO concentration of 1.5 % (from CPA #1 eluted for 15 min) led to a significant reduction in cell viability (Fig. S3E–G); whereas a residual concentration of 0.1 % did not affect cell viability, further confirming the DMSO safety threshold (<0.1 %). This finding suggests that exceeding this threshold leads to decreased cell viability. Prolonged exposure to residual DMSO (>0.1 %) has been reported to induce apoptosis and epigenetic modifications, potentially compromising *in vivo* applications [41,42]. Therefore, cryopreservation with CPA #2 and a 15-min one-step wash is selected.

3.3. Stemness and functional evaluation of cryopreserved ADSC-patch

While stem cell survival is essential, preserving their stemness and functional integrity is equally critical for clinical efficacy. We next assessed whether key stem cell functions were maintained alongside high survival rates before and after cryopreservation. The immunofluorescence staining of ADSC surface markers CD44 (positive) and CD34 (negative) confirms unaltered cell phenotype (Fig. 3A). Moreover, the stemness of ADSCs in the hydrogel patches before and after cryopreservation are examined by quantitative real-time polymerase chain

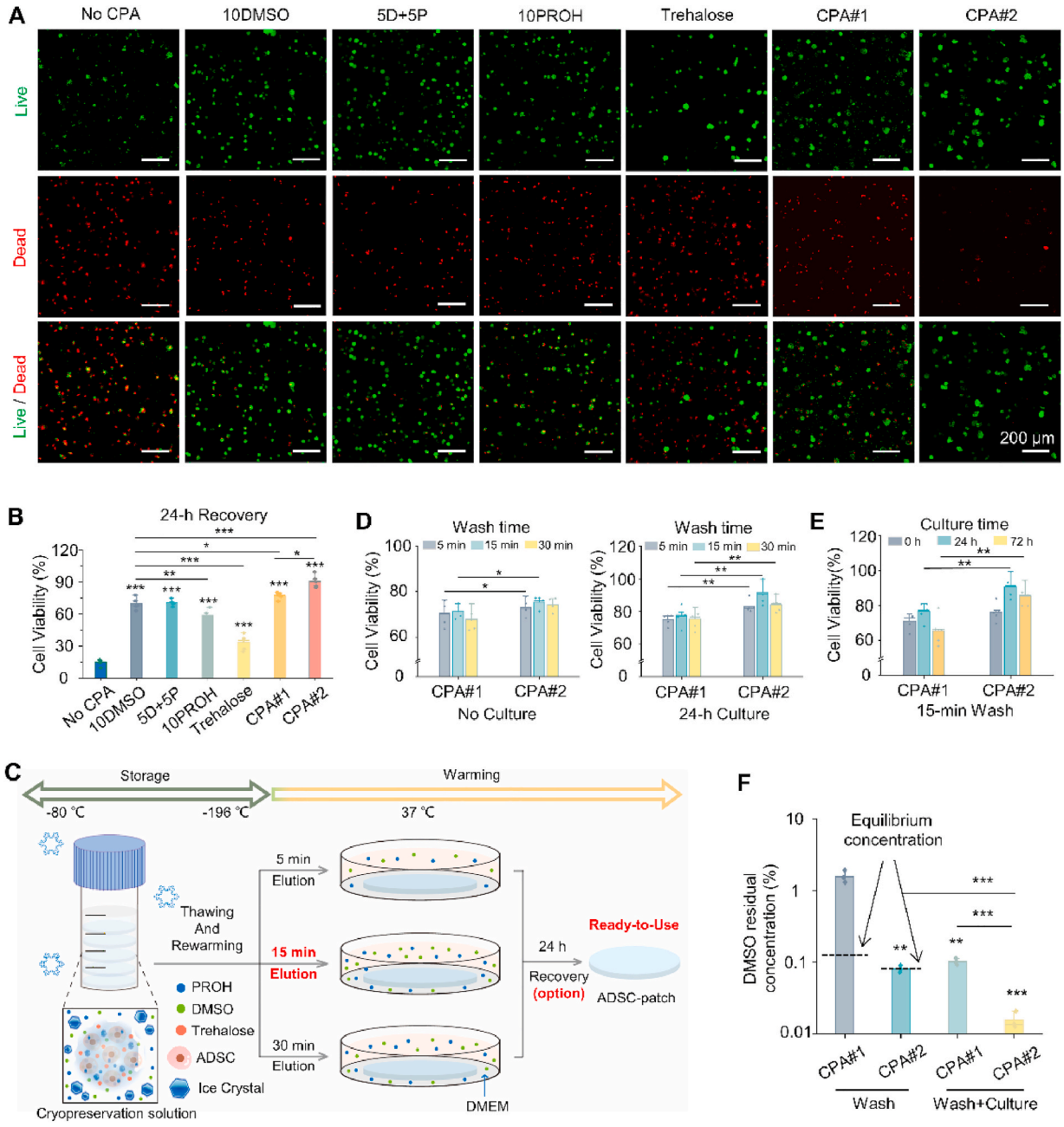

Fig. 2. Cell recovery and CPA removal post cryopreservation. (**A**) Live/dead stained fluorescent images of ADSC-patches cryopreserved with various CPA. CPA #1 and CPA #2 refer to 10 %DMSO +0.5M trehalose and 5 %DMSO +5 %PROH +0.5M trehalose, respectively. (**B**) Cell viability of ADSC-patches cryopreserved with various CPA. (**C**) Schematic representation of the elution of cryopreserved ADSC-patch after thawing. (**D**) Cell viability of cryopreserved ADSC-patches after 5-, 15- and 30-min wash and after 24-h recovery culture. (**E**) Cell viability after 15-min wash and culture of different periods (0h, 24h, 72h). (**F**) Residual concentration of DMSO in ADSC-hydrogel patches after 15-min wash and 24-h recovery culture. The dashed lines represent the equilibrium concentrations of hydrogel patches post wash (0.17 % and 0.086 % for CPA #1 and CPA #2, respectively). Independent repeat experiment n ≥ 3. *: $p < 0.05$, **: $p < 0.01$, and ***: $p < 0.001$.

reaction (qRT-PCR), and no significant differences were observed in the expression of three typical stem cell genes (KIf4, Nanog, and SOX-2) (Fig. 3B). These results suggest that Alg-DA fixation and cryopreservation maintain both cell viability and phenotype of ADSC. Next, the impact of cryopreservation on ADSC metabolic activity and cell cycle progression was evaluated. ADSC-patch remained unchanged before and after cryopreservation following 24 h of culture (Fig. S5A–C), suggesting that cryopreservation preserved the metabolic homeostasis of ADSC-patches. Furthermore, cell cycle analysis revealed a comparable distribution of ADSCs before and after cryopreservation (Fig. S5D and E), confirming that the ADSC-patch retained its functional stability and proliferative capacity.

Beyond maintaining stemness and cell phenotype, the functional capacity of the ADSC-laden patch before and after cryopreservation in promoting key regenerative processes was also evaluated. Specifically, the interaction between ADSC patches and fibroblasts (NIH/3T3), vascular endothelial cells (HUVECs) and macrophages (RAW264.7) was investigated by an *in vitro* cell co-culture system. First, transwell migration assays demonstrated that all three ADSC patch groups significantly promoted NIH/3T3 and HUVECs migration (Fig. 3C and D). In addition, ADSC-patches had higher vascularization ability as the they generated more capillary-like tubules with longer and tighter connections in Matrigel (Fig. 3E and F). The macrophage polarization ability of ADSC-patches was also tested *in vitro*. qRT-PCR results showed that

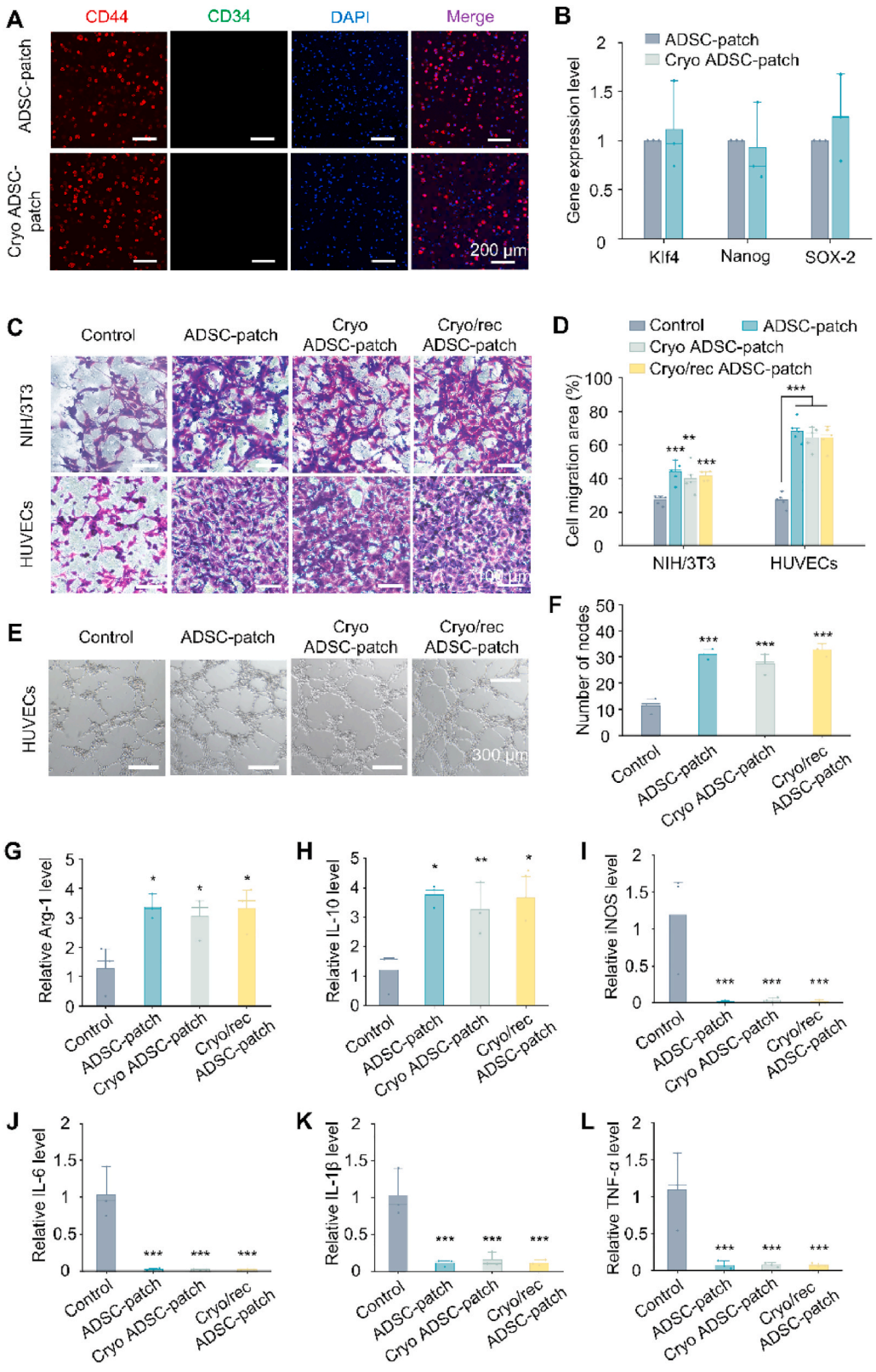

Fig. 3. Stemness and functional evaluation of cryopreserved ADSC-patch. (**A**) Immunostaining of positive CD44 (+) and negative CD34 (−) ADSCs surface markers. (**B**) Relative expressions of stem cell genes determined by qRT-PCR. (**C**) Representative images and (**D**) quantitative analysis of NIH/3T3 and HUVECs migration cocultured with ADSC-patches. (**E**) Angiogenesis assay of HUVECs cocultured with ADSC-patches. (**F**) Quantitative analysis of node number. The relative mRNA levels of (**G**) Arg-1, (**H**) IL-10, (**I**) iNOS2, (**J**) IL-6, (**K**) IL-1β and (**L**) TNF-α of macrophages cocultured with ADSC-patches. ADSC-patch, Cryo ADSC-patch and Cryo/rec ADSC-patch refers to fresh ADSC-patch, cryopreserved ADSC-patch, and cryopreserved ADSC-patch with 24-h recovery, respectively. Independent repeat experiment n ≥ 3. *: $p < 0.05$, **: $p < 0.01$, and ***: $p < 0.001$.

ADSC-patches significantly increased the expression of M2 phenotype macrophage marker genes Arg-1 and IL-10, while the inflammatory response genes of M1 macrophages, including iNOS, IL-6, IL-1β and TNF-α, showed remarkably decreased expression (Fig. 3G–L). This result confirms that the ADSC-patches, fresh or cryopreserved, can promote the conversion of M1 macrophages to M2 macrophages.

3.4. ADSC-patches heal diabetic ulcers

To test cell viability and retention of ADSC-patches before and after cryopreservation in ulcers, ADSC are transfected with Luciferase$^+$/Green fluorescent protein$^+$ (GFP) and *in vivo* bioluminescence imaging. The results indicate ADSC-patches (fresh and cryopreserved) have much longer bioluminescence (up to 7 days) than free suspended ADSCs, whose bioluminescence decreases significantly at the first 3rd hour and

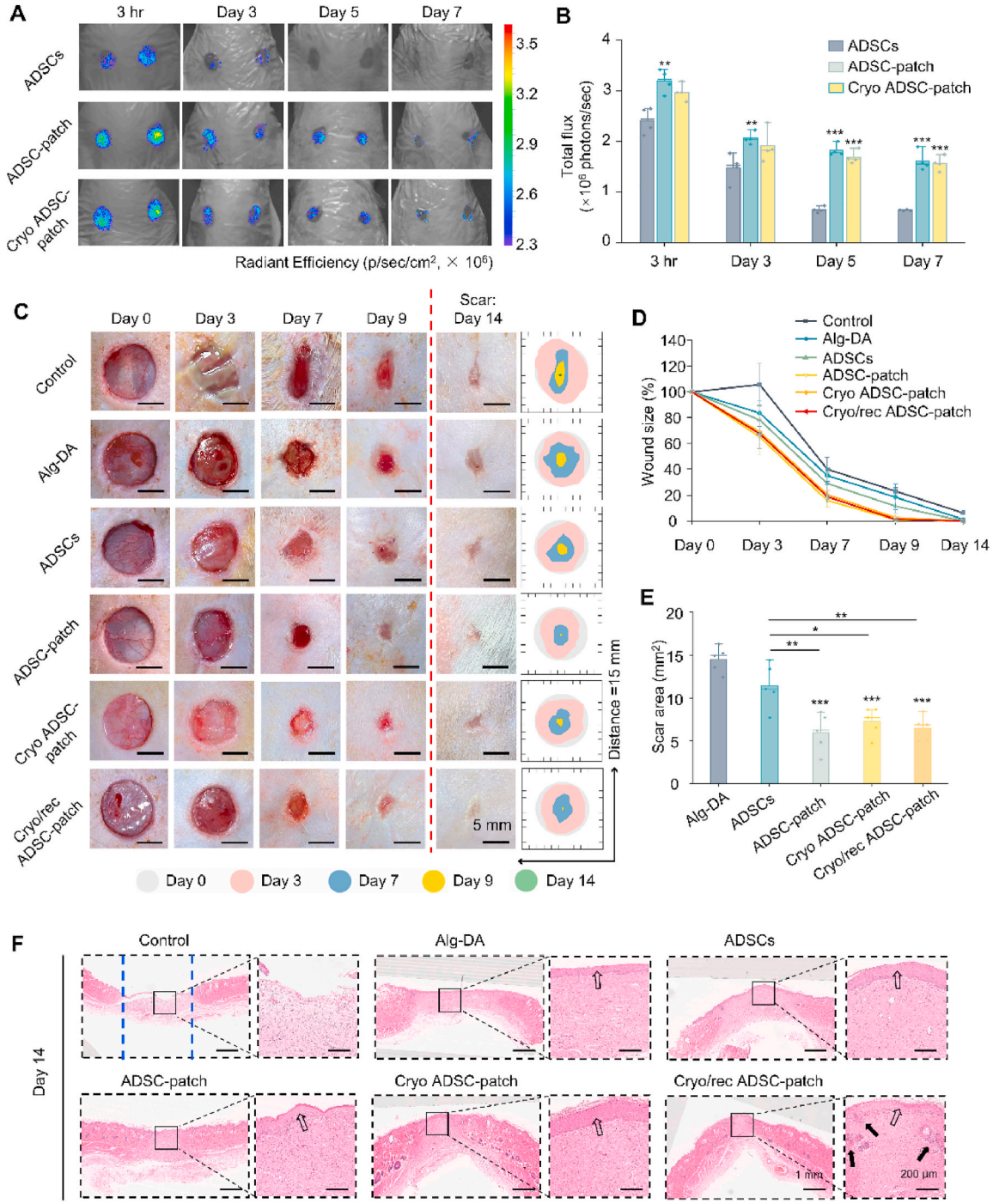

Fig. 4. Treatment of diabetic ulcers by cryopreserved ADSC-patch. (**A**) *In vivo* bioluminescence imaging, and (**B**) quantitative analysis of the Luc$^+$/GFP$^+$ ADSCs delivered by ADSC suspension, fresh and cryopreserved ADSC-patches. n = 4. (**C**) Photographs of diabetic ulcers healing of 6 groups: 1) untreated (Control); 2) hydrogel alone (Alg-DA); 3) ADSCs alone (ADSCs); 4) fresh ADSC-patch (ADSC-patch); 5) cryopreserved ADSC-patch (Cryo ADSC-patch); 6) cryopreserved ADSC-patch with 24-h recovery (Cryo/rec ADSC-patch). n = 18. (**D**) Quantitative analysis of wound size normalized to Day 0. (**E**) Quantitative analysis of scar area on Day 14. (**F**) Representative H&E stained images of diabetic ulcers on Day 14. Blue dotted line represents the unclosed area of the ulcer. Solid and open arrows respectively point to granulation and re-epithelialization in regenerated tissues. Independent repeat experiment n ≥ 3. *: $p < 0.05$, **: $p < 0.01$, and ***: $p < 0.001$.

becomes unobservable on Day 5 (Fig. 4A and B). These results prove that hydrogel patches can improve cell viability and retention in the diabetic ulcers and thus, provide long-term healing potential.

The therapeutic potential of the ADSC-patch was evaluated through diabetic ulcers in streptozotocin-induced rats. ADSC-patches (ADSC-patch, Cryo ADSC-patch and Cryo/rec ADSC-patch) only require 9 days to bring the diabetic ulcer to near complete healing, which is significantly faster than the untreated Control, Alg-DA hydrogel and ADSC suspension groups (Fig. 4C and D). The areas of healing scars are also much smaller than other groups on Day 14 (the ulcers in the untreated Control group still did not heal on Day 14) (Fig. 4C–E). Although the epidermis was not completely formed in all groups on Day 7, the three groups of ADSC-patches had higher levels of re-epithelialization and granulation (Fig. S6A). On Day 14, all groups except the Control group showed completely regenerated epidermis, and the three groups of ADSC-patches have the best recovery of granulation tissue and even presented skin appendages (Fig. 4F). Notably, the Cryo-ADSC patch demonstrates significant potential to accelerate wound healing and enhance healing quality compared to commercial Algisite™ dressings (Fig. S6B–D).

Notably, although 24-h recovery incubation *in vitro* enhances immediate cell viability (Fig. 2D), cryopreserved ADSC-patches have the same healing capacities with or without recovery, indicating ADSC in Alg-DA can recovery automatically during treatment due to the negligible DMSO residual (Fig. 2F). These results demonstrate that cryopreserved ADSC-patches can be directly utilized to treat diabetic ulcers post a simple 15-min wash without overnight recovery incubation.

3.5. Mechanistic analyses of ADSC-patch for diabetic ulcer healing

The mechanism of ADSC-patch promotion of ulcer healing was investigated on molecular (signal proteins) and histological levels. On a histological level, the masson staining showed that three ADSC-patch groups showed denser collagen deposition with more regular and orderly arrangement on both Day 7 and Day 14 (Fig. 5A and B). Particularly, they have the highest type III collagen (Col 3) concentration at the early phase but the lowest at the late phase (Fig. S7A and B), because immature Col 3 initially covers the wound to prevent damage, but excessive Col3 at late phase will lead to scar formation [43]. Notably, active angiogenesis was observed in the three ADSC patch groups by CD31 staining on day 7, whereas by day 14, the control group exhibited the most neovascularization. This could be attributed to the treatment with the ADSC patches prompting accelerated early angiogenesis to supply oxygen and nutrients, which subsequently degraded during wound remodeling as fewer vessels were needed (Fig. 5C and D). Moreover, the infiltration and polarization of macrophages at the wound site were studied by immunohistochemical staining, with all macrophages being marked by CD68 and M2 macrophages by CD163. The wounds showed higher macrophage infiltration post all treatments on Day 3 (Fig. 5E and F). Especially, the three ADSC-patch groups had more CD163 positive cells and their CD163/CD68 ratios were significantly higher than other groups, indicating that the ADSC- patches accelerate the transition from pro-inflammatory M1 to anti-inflammatory M2 macrophages (Fig. 5F). Notably, the CD163/CD68 ratios of the three ADSC-patch groups on Day 7 were similar to those on Day 3, but the CD68-positive cells decreased, which suggests the mitigation of diabetic inflammation (Fig. 5G and H).

On the level of signal proteins, ADSC-patches reduce the expression of pro-inflammatory factors (IL-6 and TNF-α) in the wounds, and promote the anti-inflammatory factor (IL-10) (Fig. 5I), proving a transition from pro-inflammatory to anti-inflammatory, tissue sparing microenvironment. VEGF-A, a key regulator of angiogenesis, stimulates vascular endothelial cells to proliferate, migrate, and form new blood vessels [44]. However, its overexpression typically leads to abnormal angiogenesis. In contrast, the ADSC patch can dynamically regulate VEGF-A expression at the wound site. Specifically, it significantly upregulated VEGF-A expression on day 7, but not on day 14 (Fig. 5I), which was consistent with the trend of CD31 expression (Fig. 5C and D). Furthermore, TGF-β1 in wound healing can promote the proliferation of dermal and epidermal cells and the production of ECM *via* inducing polarization of M2 macrophages, but its overproduction in the late stage may cause scar formation [45,46]. In consistent with accelerated wound healing and reduced scar area by ADSC-patches (Fig. 4C–E), TGF-β1 in ADSC-patch treated wounds has the highest level on Day 3 and lowest on Day 14 (Fig. 5I). Notably, WB analysis of VEGF and TNF-α exhibited trends consistent with ELISA findings on Day 14 (Fig. S7C), further corroborating the immunomodulatory and angiogenic effects mediated by the ADSC patch.

Collectively, these *in vivo* and *in vitro* mechanistic studies indicated that the ADSC-patches, fresh or cryopreserved, can accelerate wound repair and reduce scar formation by regulating inflammation, angiogenesis, collagen deposition, re-epithelialization and granulation in a concerted fashion. Specifically, in the early stage of diabetic ulcer healing, ADSC-patches reduced inflammation by promoting the conversion of M1 macrophages to M2 macrophages, downregulating pro-inflammatory IL-1β, IL-6 and TNF-α, and upregulating anti-inflammatory IL-10, VEGF, and TGF-β1. Meanwhile, the patches accelerate wound closure by enhancing angiogenesis, collagen deposition, and fibroblast migration and proliferation. In the late stage, they suppress scar formation by reducing macrophage infiltration, blood vessel formation, type III collagen deposition, and enhancing re-epithelialization and granulation at the ulcer. In addition, the ulcers were all shielded by commercial 3M Tegaderm dressing (a polyurethane film allows the transport of water vapor and oxygen but is impermeable to water and bacteria), which promotes ulcer healing and is widely used as positive controls [47,48]. Thus, the combination of exterior polyurethane films to prevent infection and interior ADSC-patches to regulate tissue regeneration is an effective approach in ulcer treatment.

3.6. ADSC-patches to treat large, shape-mismatched diabetic ulcers

Clinical diabetic ulcers vary extensively in size and shape, which often mismatch with pre-designed and pre-fabricated wound patches. To test the applicability of this ADSC-patches to heal large, shape-mismatched ulcers, we established a 2 × 3 cm full-thickness ulcer model on the dorsum of STZ-rats and covered it by arraying 8 pieces of cryopreserved ADSC-patches (Fig. 6A). The tissue-adhesiveness endowed by dopamine modification can prevent patches from sliding or displacement in the large wound bed. Compared to the untreated or hydrogel groups, ADSC-patches heal faster with smaller scar area (Fig. 6B–E and S8). For instance, the Cryo ADSC-patch groups show almost complete wound healing on Day 21, but Control and Alg-DA groups do not close their ulcers until Day 35 with significantly higher scar widths (wound edge and middle) (Fig. 6D and E). Notably, remarkable pus appears in the wound bed of Control and Alg-DA groups on Day 5, indicating much stronger inflammation than Cryo ADSC-patch groups. The Cryo ADSC-patch demonstrated an elevated CD163/CD68 ratio (Fig. 6F and G), suggesting a macrophage phenotypic shift toward the regeneration-promoting M2 type, which plays a crucial role in effective tissue repair. Additionally, collagen organization was improved in the Cryo ADSC-patch-treated group compared with the control group (Fig. 6H and I), and the Col 1/Col 3 ratio was significantly lower (Fig. 6J and K), suggesting reduced fibrotic scarring and enhanced regenerative healing potential. Therefore, the ADSC-patches produce minimum scar area with smallest granulation gaps and most mature tissues of healthy skin.

4. Discussion

The thin cell-laden patch reported here was fabricated through simple, reusable PDMS molds with short turnover time (<15 min). In addition, the fabrication only uses simple materials and equipment,

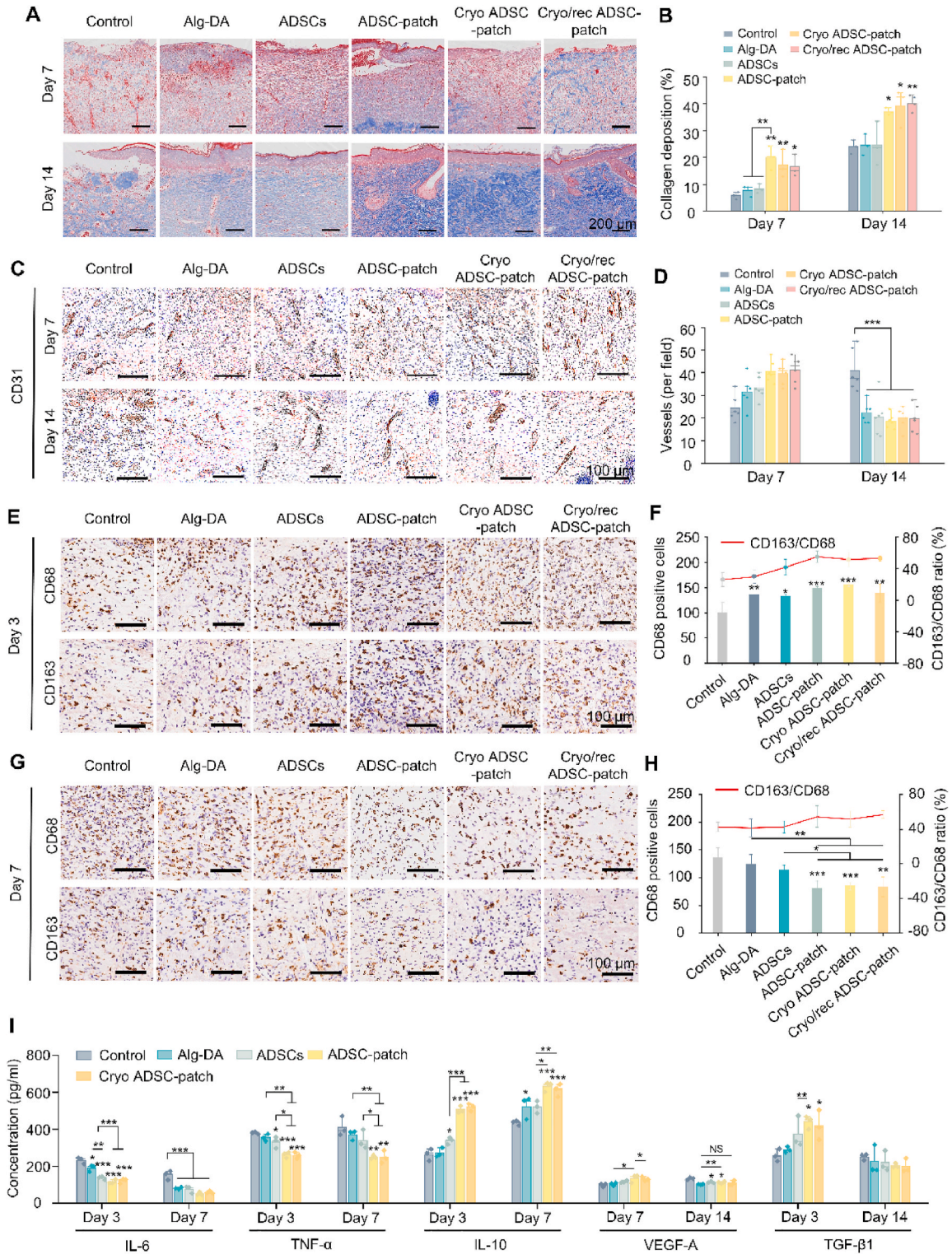

Fig. 5. Mechanistic studies of ADSC-patch for healing diabetic ulcers. (**A**) Representative images of Masson's staining at ulcers on Day 7 and Day 14. (**B**) Quantitative analysis of collagen deposition. (**C**) Representative images and (**D**) quantitative analysis of CD31 (brown) immunochemical (IHC) staining at ulcers on Day 7 and Day 14. (**E**) Representative images of CD68 and CD163 (brown) IHC staining at ulcers on Day 3. (**F**) Quantitative analysis of normalized CD68 and CD163/CD68 ratio on Day 3. (**G**) Representative images of CD68 and CD163 (brown) IHC staining at ulcers on Day 7. (**H**) Quantitative analysis of normalized CD68 and CD163/CD68 ratio on Day 7. (**I**) Levels of IL-6, TNF-α, IL-10, VEGF-A and TGF-β1 in wound tissue during healing process measured by ELISA. Independent repeat experiment n ≥ 3. *: $p < 0.05$, **: $p < 0.01$, and ***: $p < 0.001$.

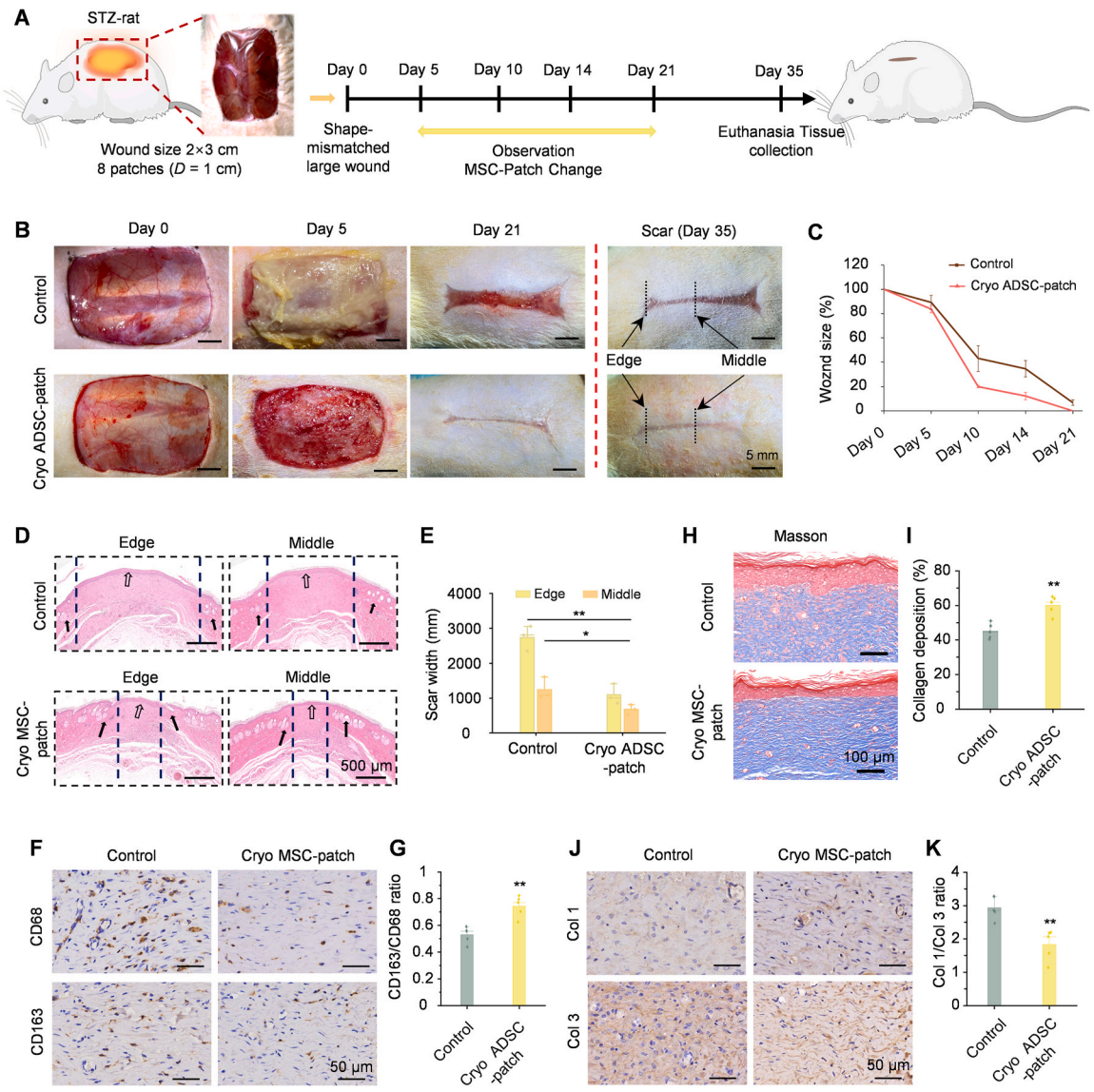

Fig. 6. Large, shape-mismatched ulcer treated by assembling cryopreserved ADSC-patch. (**A**) Schematic diagram of the experimental duration of ADSC-patch for the treatment of 2 × 3 cm square-shaped diabetic ulcer in STZ-rat. (**B**) Photograph and (**C**) corresponding wound size of large ulcers treated with control and Cryo ADSC-patch on different days. (**D**) Representative H&E stained images of ulcers on Day 35. Solid and open arrows respectively point to granulation and re-epithelialization in closed wounds. (**E**) Quantitative analysis of scar width (edge and middle) on Day 35. (**F**) Representative images of CD68 and CD163 (brown) IHC staining on Day 35. (**G**) Quantitative analysis of CD163/CD68 ratio. (**H**) Representative images of Masson's staining at ulcers on Day 35. (**I**) Quantitative analysis of collagen deposition. (**E**) Representative images of Col 1 and Col 3 (brown) IHC staining on Day 35. (**F**) Quantitative analysis of Col 1/Col 3 ratio. n = 3. *: $p < 0.05$, **: $p < 0.01$.

allowing economic mass-production. Moreover, the thin, pancake shape of the patch offers multiple advantages: (1) minimizing material consumptions in manufacturing, preventing structure heterogeneity during gelation, and reducing waste generation post usage, (2) enabling energy-efficient packaging, cryopreservation, and transportation in-stack manner, (3) enabling close cell contact and fast cellular response to ever changing ulcer microenvironments, (4) facilitating fast CPA loading and unloading with reduced wash time at the user end. The low-cost, environmentally friendly, and user-friendly characteristics render this cell-laden patch well-suited for broad clinical adoption.

Cryopreservation of macroscale cell-laden patches is a major hurdle in the supply chain for its widespread distribution. The large size of cell-laden constructs not only causes heterogeneities of temperature and CPA distributions within constructs during cooling and warming procedures of cryopreservation, but also impedes the removal of cryoprotective agents such as DMSO and serum. High level of serum and DMSO residuals would cause severe conditions such as fever and hypersensitivity in patients [13,49,50], while extended wash to remove cytotoxic cryoprotectants induces irreversible cell damages (Fig. 2E). By combining the strategies of *p*CPA, *n*CPA, and thin-pancaked shape of cell-patches, the residual DMSO in macroscale patches was reduced to a noncytotoxic level with a short, simple 15-min wash. In addition, the production, cryopreservation, and wash medium for cell-laden patches are DMEM-based solutions without serum. This not only ensures the consistency and reproducibility of fabrication and application due to the fully defined and characterized solution components, but also reduces the immune responses from the transplant host.

Scalabilities in production, storage, and clinic utilization are critical factors to the success of cell-biomaterial constructs. The cell-laden patch reported here can be efficiently fabricated and cryopreserved in a high-throughput, batch production format, offering a practical, ready-to-use solution tailored to clinical needs. Its scalable and flexible design

enables straightforward assembly to accommodate variable sizes and shapes of diabetic ulcers. Importantly, the patch preserves stem cell viability, functionality, and retention rates during *in vitro* storage and *in vivo* transplantation. With its simplified preparation process, requiring only a simple 15-min wash with no specialized equipment or personnel needed, this patch substantially streamlines preclinical and clinical workflows.

The thin ADSC-patch is well-suited for application on irregularly shaped wounds (Fig. 6A), allowing for easy stacking and providing personalized treatment options tailored to individual patient needs. The ADSC-patch dynamically responds to the changing inflammatory microenvironment of diabetic ulcers, promoting wound healing through long-term, multifaceted self-regulation of paracrine secretion, macrophage polarization, and angiogenesis. In the early healing stage, ADSC-patch convert pro-inflammatory M1 to anti-inflammatory M2 macrophages, downregulate pro-inflammatory IL-1β, IL-6 and TNF-α, and upregulate anti-inflammatory IL-10, VEGF-A, and TGF-β1. In the late stage, ADSC-patch suppress inflammatory response by inhibiting macrophage infiltration, and thus, reducing blood vessel formation, Col3 deposition, and scar formation (Fig. 5). The dynamics of these phenotypic results suggest that ADSC patches may coordinate the healing process through stage-specific signaling pathways: (1) NF-κB inhibition and STAT3 activation polarize macrophages to an M2 phenotype [51,52], thereby attenuating inflammation; (2) PI3K/Akt-driven secretion of vascular endothelial growth factor transiently enhances angiogenesis [53]; and (3) TGF-β/SMAD dynamics balance early ECM synthesis with late-stage fibrosis inhibition [52]. Therefore, this stem cell-laden patch provides a safe, effective, convenient method to clinically treat ulcers.

Overall, the ADSC-patch addresses a critical unmet need in diabetic ulcer therapies. For example, whereas current bioengineered skin substitutes (e.g., Dermagraft®) rely on costly neonatal foreskin fibroblasts and lengthy production cycles, and exosome-based hydrogels suffer from batch-to-batch variability and static therapeutic profiles, the ADSC-patch integrates three major innovations: (1) a cost-effective, scalable production process that enables widespread clinical adoption, (2) an optimized cryopreservation protocol that ensures greater than 90 % cell survival after thawing while maintaining low DMSO residues, and (3) dynamic bioactivity driven by living ADSCs, which continuously modulate inflammation, angiogenesis, and ECM remodeling through stage-specific paracrine signaling. Furthermore, the modular, ready-to-use design of the ADSC-patch improves its clinical applicability. Unlike traditional cell therapies that require on-demand preparation and immediate application, the cryopreserved ADSC-patch maintains stability at −80 °C for long-term storage and preserves its therapeutic efficacy following rapid thawing. Additionally, its tissue-adhesive hydrogel matrix ensures secure wound coverage without the need for external fixation, while its scalable batch fabrication streamlines manufacturing while reducing complexity and cost, making it an economically viable solution for both high-resource and resource-limited healthcare settings. Finally, the principles demonstrated in this study-integrating scalable fabrication, optimized cryopreservation, and streamlined clinical workflows-offer a robust framework for the development of other cell-biomaterial constructs to tackle diverse medical conditions such as ischemic injuries, endocrine disorders, and autoimmune diseases.

5. Conclusions

This study provides a cryopreservable, scalable, ready-to-use ADSC-loaded alginate-dopamine hydrogel patch with significant clinical applicability. Through optimization of the cryopreservation strategy using a cocktail of DMSO, PROH, and trehalose, combined with a thin, flexible patch design, we ensured high cell viability and minimal residual toxicity post-thaw. This approach eliminates the need for complex preparation steps, facilitating direct use after cryopreservation without the need for centrifugation or incubation. The tissue-adhesive patch maintains close contact with diabetic wounds, promoting rapid cellular responses and dynamic paracrine signaling that modulate inflammation, angiogenesis, and wound healing. In conclusion, we present a cost-effective, ready-to-use solution for cell therapy with scalable clinical potential and promising broader applications in regenerative medicine.

CRediT authorship contribution statement

Bangrui Yu: Writing – original draft, Visualization, Validation, Methodology, Investigation, Formal analysis, Data curation, Conceptualization. **Lanlan Peng:** Validation, Methodology. **Wenjun Dang:** Validation, Methodology. **Ying Fu:** Validation, Methodology. **Zhijie Li:** Validation, Methodology. **Jinteng Feng:** Validation, Methodology. **Heng Zhao:** Validation, Methodology. **Tian Wang:** Validation, Methodology. **Feng Xu:** Writing – review & editing. **Martin L. Yarmush:** Writing – review & editing. **Haishui Huang:** Writing – review & editing, Visualization, Supervision, Resources, Project administration, Funding acquisition, Conceptualization.

Ethics approval and consent to participate

All experimental procedures involving animals were approved by Xi'an Jiaotong University, School of Life Science and Technology (Xi'an, China) ((2023) No. 4).

Declaration of competing interest

The authors declare the following financial interests/personal relationships which may be considered as potential competing interests: Haishui huang has patent licensed to Xi'an Jiaotong University. H.H. and B.Y. have provisional patent applications relevant to this study. If there are other authors, they declare that they have no known competing financial interests or personal relationships that could have appeared to influence the work reported in this paper.

Acknowledgements

This work was supported by the National Natural Science Foundation of China (Grant No. GYKP019, 52076157), and Xian Jiaotong University (Young Talent Support Program).

Appendix A. Supplementary data

Supplementary data to this article can be found online at https://doi.org/10.1016/j.bioactmat.2025.04.024.

Data availability

Data will be made available on request.

References

[1] E.A. Kimbrel, R. Lanza, Next-generation stem cells—ushering in a new era of cell-based therapies, Nat. Rev. Drug Discov. 19 (7) (2020) 463–479.
[2] M. De Luca, A. Aiuti, G. Cossu, M. Parmar, G. Pellegrini, P.G. Robey, Advances in stem cell research and therapeutic development, Nat. Cell Biol. 21 (7) (2019) 801–811.
[3] J.S. Hyun, M.C. Tran, V.W. Wong, M.T. Chung, D.D. Lo, D.T. Montoro, D.C. Wan, M.T. Longaker, Enhancing stem cell survival in vivo for tissue repair, Biotechnol. Adv. 31 (5) (2013) 736–743.
[4] Y. Li, Y. Xiang, Y. Chen, Y. Wang, W. Dong, Y. Liu, X. Qi, J. Shen, A natural eumelanin-assisted pullulan/chitosan hydrogel for the management of diabetic oral ulcers, Macromol. Biosci. 25 (3) (2025) 2400526.
[5] Y. Xiang, Z. Pan, X. Qi, X. Ge, J. Xiang, H. Xu, E. Cai, Y. Lan, X. Chen, Y. Li, A cuttlefish ink nanoparticle-reinforced biopolymer hydrogel with robust adhesive and immunomodulatory features for treating oral ulcers in diabetes, Bioact. Mater. 39 (2024) 562–581.
[6] M.P. Lutolf, P.M. Gilbert, H.M. Blau, Designing materials to direct stem-cell fate, Nature 462 (7272) (2009) 433–441.

[7] J.A. Burdick, R.L. Mauck, S. Gerecht, To serve and protect: hydrogels to improve stem cell-based therapies, Cell Stem Cell 18 (1) (2016) 13–15.
[8] C.M. Madl, S.C. Heilshorn, H.M. Blau, Bioengineering strategies to accelerate stem cell therapeutics, Nature 557 (7705) (2018) 335–342.
[9] O. Chaudhuri, L. Gu, D. Klumpers, M. Darnell, S.A. Bencherif, J.C. Weaver, N. Huebsch, H.-p. Lee, E. Lippens, G.N. Duda, Hydrogels with tunable stress relaxation regulate stem cell fate and activity, Nat. Mater. 15 (3) (2016) 326–334.
[10] N. Mitrousis, A. Fokina, M.S. Shoichet, Biomaterials for cell transplantation, Nat. Rev. Mater. 3 (11) (2018) 441–456.
[11] H. Huang, X. He, M.L. Yarmush, Advanced technologies for the preservation of mammalian biospecimens, Nat. Biomed. Eng. 5 (8) (2021) 793–804.
[12] B.P. Best, Cryoprotectant toxicity: facts, issues, and questions, Rejuvenation Res. 18 (5) (2015) 422–436.
[13] P. Windrum, T. Morris, M. Drake, D. Niederwieser, T. Ruutu, Variation in dimethyl sulfoxide use in stem cell transplantation: a survey of EBMT centres, Bone Marrow Transplant. 36 (7) (2005) 601–603.
[14] K.A. Murray, R.M. Tomás, M.I. Gibson, Low DMSO cryopreservation of stem cells enabled by macromolecular cryoprotectants, ACS Appl. Bio Mater. 3 (9) (2020) 5627–5632.
[15] D.E. Pegg, Principles of Cryopreservation, Cryopreservation and Freeze-Drying Protocols, 2007, pp. 39–57.
[16] H. Huang, J.K. Choi, W. Rao, S. Zhao, P. Agarwal, G. Zhao, X. He, Alginate hydrogel microencapsulation inhibits devitrification and enables large-volume low-CPA cell vitrification, Adv. Funct. Mater. 25 (44) (2015) 6839–6850.
[17] H. Gurruchaga, L.S. Del Burgo, R. Hernandez, G. Orive, C. Selden, B. Fuller, J. Ciriza, J. Pedraz, Advances in the slow freezing cryopreservation of microencapsulated cells, J. Contr. Release 281 (2018) 119–138.
[18] T. Chang, G. Zhao, Ice inhibition for cryopreservation: materials, strategies, and challenges, Adv. Sci. 8 (6) (2021) 2002425.
[19] H. Huang, M.L. Yarmush, O.B. Usta, Long-term deep-supercooling of large-volume water and red cell suspensions via surface sealing with immiscible liquids, Nat. Commun. 9 (1) (2018) 1–10.
[20] S. Freitas-Ribeiro, A.F. Carvalho, M. Costa, M.T. Cerqueira, A.P. Marques, R.L. Reis, R.P. Pirraco, Strategies for the hypothermic preservation of cell sheets of human adipose stem cells, PLoS One 14 (10) (2019) e0222597.
[21] S. Freitas-Ribeiro, A.F. Carvalho, D.B. Rodrigues, L. Martins, R.A. Pires, V. M. Mendes, B. Manadas, M. Jarnalo, R. Horta, R.L. Reis, Cryogenic, but not hypothermic, preservation disrupts the extracellular matrix of cell sheets, Bioact. Mater. 46 (2025) 301–310.
[22] L. Weng, P.R. Beauchesne, Dimethyl sulfoxide-free cryopreservation for cell therapy: a review, Cryobiology 94 (2020) 9–17.
[23] C.-C. Chang, L.-Y. Sung, C.-J. Lin, H.I. Kort, X. Yang, X.C. Tian, Z.P. Nagy, The oocyte spindle is preserved by 1, 2-propanediol during slow freezing, Fertil. Steril. 93 (5) (2010) 1430–1439.
[24] H. Huang, G. Zhao, Y. Zhang, J. Xu, T.L. Toth, X. He, Predehydration and ice seeding in the presence of trehalose enable cell cryopreservation, ACS Biomater. Sci. Eng. 3 (8) (2017) 1758–1768.
[25] K.A. Murray, M.I. Gibson, Chemical approaches to cryopreservation, Nat. Rev. Chem 6 (8) (2022) 579–593.
[26] V. Falanga, R.R. Isseroff, A.M. Soulika, M. Romanelli, D. Margolis, S. Kapp, M. Granick, K. Harding, Chronic wounds, Nat. Rev. Dis. Primers 8 (1) (2022) 50.
[27] M. Kharaziha, A. Baidya, N. Annabi, Rational design of immunomodulatory hydrogels for chronic wound healing, Adv. Mater. 33 (39) (2021) 2100176.
[28] S. Dhivya, V.V. Padma, E. Santhini, Wound dressings–a review, Biomedicine 5 (4) (2015) 1–5.
[29] S. Matoori, A. Veves, D.J. Mooney, Advanced bandages for diabetic wound healing, Sci. Transl. Med. 13 (585) (2021) eabe4839.
[30] S.-R. Park, J.-W. Kim, H.-S. Jun, J.Y. Roh, H.-Y. Lee, I.-S. Hong, Stem cell secretome and its effect on cellular mechanisms relevant to wound healing, Mol. Ther. 26 (2) (2018) 606–617.
[31] N. Song, M. Scholtemeijer, K. Shah, Mesenchymal stem cell immunomodulation: mechanisms and therapeutic potential, Trends Pharmacol. Sci. 41 (9) (2020) 653–664.
[32] M.M. Hasani-Sadrabadi, P. Sarrion, S. Pouraghaei, Y. Chau, S. Ansari, S. Li, T. Aghaloo, A. Moshaverinia, An engineered cell-laden adhesive hydrogel promotes craniofacial bone tissue regeneration in rats, Sci. Transl. Med. 12 (534) (2020) eaay6853.
[33] O. Davies, A. Smith, P. Cooper, R. Shelton, B. Scheven, The effects of cryopreservation on cells isolated from adipose, bone marrow and dental pulp tissues, Cryobiology 69 (2) (2014) 342–347.
[34] J. Gan, C. Liu, H. Li, S. Wang, Z. Wang, Z. Kang, Z. Huang, J. Zhang, C. Wang, D. Lv, Accelerated wound healing in diabetes by reprogramming the macrophages with particle-induced clustering of the mannose receptors, Biomaterials 219 (2019) 119340.
[35] A. GhavamiNejad, J. Li, B. Lu, L. Zhou, L. Lam, A. Giacca, X.Y. Wu, Glucose-responsive composite microneedle patch for hypoglycemia-triggered delivery of native glucagon, Adv. Mater. 31 (30) (2019) 1901051.
[36] T. Priemel, G. Palia, F. Förste, F. Jehle, S. Sviben, I. Mantouvalou, P. Zaslansky, L. Bertinetti, M.J. Harrington, Microfluidic-like fabrication of metal ion–cured bioadhesives by mussels, Science 374 (6564) (2021) 206–211.
[37] K. Liu, X. Dong, Y. Wang, X. Wu, H. Dai, Dopamine-modified chitosan hydrogel for spinal cord injury, Carbohydr. Polym. 298 (2022) 120047.
[38] P. Samyn, A platform for functionalization of cellulose, chitin/chitosan, alginate with polydopamine: a review on fundamentals and technical applications, Int. J. Biol. Macromol. 178 (2021) 71–93.
[39] M. Klontzas, H. Drissi, A. Mantalaris, The use of alginate hydrogels for the culture of mesenchymal stem cells (MSCs): in vitro and in vivo paradigms, in: L. Pereira (Ed.), Alginates—Recent Uses of This Natural Polymer, 2020, pp. 65–80.
[40] A. Bissoyi, B. Nayak, K. Pramanik, S.K. Sarangi, Targeting cryopreservation-induced cell death: a review, Biopreserv. Biobanking 12 (1) (2014) 23–34.
[41] J. Galvao, B. Davis, M. Tilley, E. Normando, M.R. Duchen, M.F. Cordeiro, Unexpected low-dose toxicity of the universal solvent DMSO, FASEB J. 28 (3) (2014) 1317–1330.
[42] M. Verheijen, M. Lienhard, Y. Schrooders, O. Clayton, R. Nudischer, S. Boerno, B. Timmermann, N. Selevsek, R. Schlapbach, H. Gmuender, DMSO induces drastic changes in human cellular processes and epigenetic landscape in vitro, Sci. Rep. 9 (1) (2019) 4641.
[43] S.W. Volk, Y. Wang, E.A. Mauldin, K.W. Liechty, S.L. Adams, Diminished type III collagen promotes myofibroblast differentiation and increases scar deposition in cutaneous wound healing, Cells Tissues Organs 194 (1) (2011) 25–37.
[44] A. King, S. Balaji, S.G. Keswani, T.M. Crombleholme, The role of stem cells in wound angiogenesis, Adv. Wound Care 3 (10) (2014) 614–625.
[45] J. Zhang, Y. Zheng, J. Lee, J. Hua, S. Li, A. Panchamukhi, J. Yue, X. Gou, Z. Xia, L. Zhu, A pulsatile release platform based on photo-induced imine-crosslinking hydrogel promotes scarless wound healing, Nat. Commun. 12 (1) (2021) 1–13.
[46] S.R. Beanes, C. Dang, C. Soo, K. Ting, Skin repair and scar formation: the central role of TGF-β, Expet Rev. Mol. Med. 5 (8) (2003) 1–22.
[47] K. Skórkowska-Telichowska, M. Czemplik, A. Kulma, J. Szopa, The local treatment and available dressings designed for chronic wounds, J. Am. Acad. Dermatol. 68 (4) (2013) e117–e126.
[48] D.R. Griffin, M.M. Archang, C.-H. Kuan, W.M. Weaver, J.S. Weinstein, A.C. Feng, A. Ruccia, E. Sideris, V. Ragkousis, J. Koh, Activating an adaptive immune response from a hydrogel scaffold imparts regenerative wound healing, Nat. Mater. 20 (4) (2021) 560–569.
[49] C.E. Goldring, P.A. Duffy, N. Benvenisty, P.W. Andrews, U. Ben-David, R. Eakins, N. French, N.A. Hanley, L. Kelly, N.R. Kitteringham, Assessing the safety of stem cell therapeutics, Cell Stem Cell 8 (6) (2011) 618–628.
[50] C.A. Herberts, M.S. Kwa, H.P. Hermsen, Risk factors in the development of stem cell therapy, J. Transl. Med. 9 (1) (2011) 1–14.
[51] Z. Dong, Y. Fu, Z. Cai, H. Dai, Y. He, Recent advances in adipose-derived mesenchymal stem cell-derived exosomes for regulating macrophage polarization, Front. Immunol. 16 (2025) 1525466.
[52] L. Mazini, L. Rochette, B. Admou, S. Amal, G. Malka, Hopes and limits of adipose-derived stem cells (ADSCs) and mesenchymal stem cells (MSCs) in wound healing, Int. J. Mol. Sci. 21 (4) (2020) 1306.
[53] J. Wang, H. Wu, Y. Peng, Y. Zhao, Y. Qin, Y. Zhang, Z. Xiao, Hypoxia adipose stem cell-derived exosomes promote high-quality healing of diabetic wound involves activation of PI3K/Akt pathways, J. Nanobiotechnol. 19 (2021) 1–13.